https://doi.org/10.3311/PPci.22020
Creative Commons Attribution

Periodica Polytechnica Civil Engineering, 68(1), pp. 337–348, 2024

Cyclic Behavior of New Steel Plate Shear Walls Reinforced with Trapezoidal Corrugated Plates

Seyedeh Maryam Dashti Zand[1], Vahidreza Kalatjari[1], Nader. K. A. Attari[2*]

[1] Civil Engineering Department, Shahrood University of Technology, 3619995161, Shahrood, Iran
[2] Structural Engineering Department, Road, Housing and Urban Development Research Center (BHRC), 1463917151, Tehran, Iran
[*] Corresponding author, e-mail: n.attari@bhrc.ac.ir

Received: 08 February 2023, Accepted: 21 September 2023, Published online: 17 October 2023

Abstract

Unstiffened steel plate shear walls have low buckling strength, which caused development diagonal tension field under lateral load. Corrugated plates have higher out-of-plane stiffness and improved buckling stability. Combining corrugated and flat plates in steel shear wall web could be effective. In this paper a new steel shear wall system reinforced with trapezoidal corrugated steel plates were proposed. In this study, the behavior of the system was experimentally studied under cyclic loading. Four specimens with the one-third scale were evaluated, which were control unstiffened specimen, the specimen with vertical 45° trapezoidal corrugated web, specimen with a corrugated web plate reinforced with two flat plates, and specimen with a flat web plate reinforced with two corrugated plates. In all four specimens, the total thicknesses of steel plates were the same; therefore, the thickness of each plate in specimens with three plates was one-third of the specimen with one plate. The studied parameters were the bearing capacity, maximum base shear, stiffness, ductility, energy absorption, and modification factor for the dissipation capacity of the specimens. The results revealed the maximum lateral load capacity of specimen with a flat web plate reinforced with two corrugated plates increased about 17%, 37%, and 19%, comparly to unstiffened specimens, vertical 45° trapezoidal corrugated web, and corrugated web plate reinforced with two flat plates, respectively. According to the results, the behavior of the seismic parameters of the proposed specimen with a flat web plate reinforced with two corrugated plates was clearly better than that of the other specimens.

Keywords

cyclic loading, experimental test, steel plate shear wall, trapezoidal-corrugated steel plate shear wall

1 Introduction

In the last three decades, the steel plate shear wall (SPSW) has been used as a lateral load-bearing system in earthquake-prone countries [1]. The most common type of SPSW in most countries is the thin-web unstiffened SPSW, which is a special steel plate shear wall (SSPSW) system known in ASCE/SEI 7-10 [2] and ANSI/AISC 341-10 [3] as a basic seismic-resistant system. In steel shear walls, this type of wall has a low compressive strength due to its high slenderness ratio; therefore, it experiences diagonal shear buckling in the web plate when subjected to a small earthquake-induced shear force. The second type of lateral load-bearing system is the stiffened steel shear wall in which the shear buckling strength of the web plate is increased by adding a stiffener, improving the structural system's rigidity, energy absorption, and hysteresis behavior. Although using stiffeners in steel shear walls is quite common, using walls stiffened with many stiffeners has many disadvantages, such as more construction time, increased steel consumption, and increased in structure weight [4]. The steel corrugated plate shear walls (SCPSWs) have been widely employed in multi-story or high-rise building structures. Trapezoidal corrugated plates have special geometry and high out-of-plane stiffness; thus, they have much higher buckling strength than flat plates because of their multiple bends converted in-plane forces to out-of-plane ones in this system the required web thickness were red need and the stiffener's is not required in this system. This type of wall has advantages over stiffened and unstiffened shear walls because that the corrugated plate's stiffness eliminates problems related to out-of-plane and costs due to eliminating the stiffeners [5–8]. SCPSWs commonly have boundary beams and columns using welded or bolted connections [9–11]. Over the past decades, numerous investigations have been conducted on

Cite this article as: Zand, S. M. D., Kalatjari V., Attari, N. K. A. "Cyclic Behavior of New Steel Plate Shear Walls Reinforced with Trapezoidal Corrugated Plates", Periodica Polytechnica Civil Engineering, 68(1), pp. 337–348, 2024. https://doi.org/10.3311/PPci.22020

the behavior and design of the SCPSWs [12–26]. Among them, the elastic buckling, load resistance, and hysteretic behaviors of SCPSWs under in-plane shear loads were comprehensively evaluated, which can provide valuable references for the design of SCPSWs in practice [8]. Guo et al. [27] and Zhu et al. [28] investigated the compression performance of the corrugated steel plate composite wall. The formula for calculating the ultimate load capacity was derived by fitting the correlation curves of the normalized slenderness ratio and stability coefficient. Further, Jiang et al. [29] proposed a new special steel frame with stiffened double SPSW. The experimental results demonstrated that the buckling of steel faceplates and overall instability of the wall were the main failure modes of the SDSPSW. Tong et al. [30] also studied double-corrugated-plate shear walls (DCPSWs), composed of two identical corrugated plates assembled by connecting bolts. Based on the results, the ultimate shear resistance of DCPSWs increased with the increase of the aspect ratio, bolt numbers, and corrugation amplitude; nonetheless, the dimensions of the boundary elements had little effect on the shear resistance of the embedded corrugated plates.

In recent years, to fulfill the requirements of high-rise building structures, the SCPSWs were trending to a higher load-resistant design. Considering the special trapezoidal shape and high out-of-plane stiffness of corrugated plates and their three types of buckling (local, regional, and general buckling), both corrugated steel shear walls and flat stiffened systems can increase the structural stiffness. However, they represent weaker performance than unstiffened steel shear walls in the seismic behavior, ultimate strength, and energy absorption [5–8]. Accordingly, considering that both flat and corrugated plates have advantages and disadvantages in terms of providing seismic parameters, the present study proposed and examined a system of combined flat and corrugated plates that uses the advantages of both plates to improve the performance of SPSWs.

Four specimens were tested in this study, which were, the control unstiffened specimen (SPSW), the specimen with vertical 45° trapezoidal corrugated web (CSPSW), the specimen with a corrugated web plate reinforced with two flat plates (SCSSPWs), and the specimen with a flat web plate reinforced with two corrugated plates (CSCSPWs). All samples were of a one-story frame with a 1:3 scale and had similar total web-plate thickness (1.5 mm) and same boundary elements and joints. All specimens were clamped to the floor, and all horizontal boundary elements (HBE) to vertical boundary elements (VBE) joints were designed as rigid connections. The tests were based on methods approved for simulating seismic loads and were performed under quasi-static cyclic loading [31]. The elastic/inelastic resistance, stiffness, ductility, and energy absorption of the specimens were compared with each other's.

2 Materials and methods

2.1 Specimen specifications

The experimental program consisted of four 1:3 scale SPSW with different types of plates and details. The tests were performed at the Building and Housing Research Center (BHRC) laboratory. Specimen 1 was an unstiffened thin web-plate SPSW with 1.5 mm thickness (Fig. 1(a)). Specimen 2 was a corrugated steel plate shear wall (CSPSW) with a vertical 45º trapezoidal plate and 1.5 mm thickness (Fig. 1(b)). Specimen 3 consisted of one vertical 45º trapezoidal corrugated plate with 0.5 mm thickness in the middle and two flat plates on its both sides (SCSSPSW). Due to the low web-plate thickness (0.5 mm), a special CO_2 welding method and 4 mm fishplate were used to connect each of the two flat web plates to the boundary element frame. The two flat plates were connected to the trapezoidal plate using No. 5 self-tapping screws. The minimum center-to-center distance of the screws, as well as the minimum screw distance from the edge, were three times the nominal diameter of the screw (Fig. 1(c)) [32]. Specimen 4 included two vertical 45º trapezoidal corrugated plates

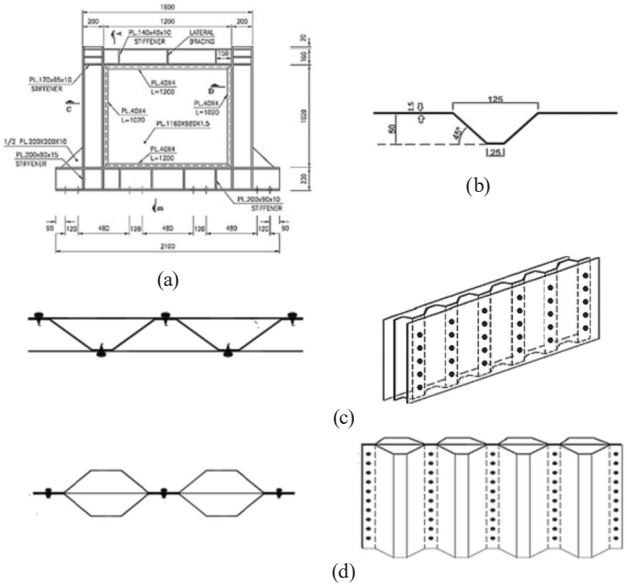

Fig. 1 Specification of specimens: Specification of the (a) frames (horizontal boundary elements (HBEs) and vertical boundary elements (VBEs) specimens and web-plate of the SPSW specimen (mm), (b) web-plate of the CSPSW specimen (mm), (c) web-plate of the SCSSPSW specimen, and (d) web-plate of the CSCSPSW specimen

with 0.5 mm thickness on the sides and one flat plate with a 0.5 mm thickness plate in the middle (CSCSPSW). A 4 mm fishplate was used to connect the flat steel plate to boundary elements. The webs of flat and two trapezoidal corrugated plates were connected by No. 8 bolts and nuts at distances of 40 mm and 50 mm in vertical and horizontal directions, respectively, No. 10 bolts and nuts were employed to connect all three web plates to the fishplate. Also, two washers were utilized on the sides of the bolts to prevent plates tearing due to their low thickness. The flat web plate was connected to the fish plate using the CO_2 welding method due to its low thickness (0.5 mm) according to (Fig. 1(d)).

In this study, the boundary elements of the special steel shear wall with flat, unstiffened plates are designed according to AISC design guide 20 [33], and the same boundary elements were used for the other shear walls to compare their seismic performance. The nominal shear force applied to the web plate was as follows:

$$V_n = 0.42 f_y t_w L_{cf} \sin 2\alpha \ . \quad (1)$$

Where f_y, t_w, L_{cf}, and α represented the steel yield strength, the web-plate thickness, the beam free length (the distance between two column sides), and the inclination angle of the diagonal tensile field, respectively. To find α, it is necessary to have the initial size and dimensions of VBEs and HBEs, determined based on the assumptions made for the bearing of the forces created in them. For the initial design, it was assumed that the web plate resisted the entire system's shear and the tensile stress angle, which varied between 30 and 60°, was 450 [33]. The minimum moment of the inertia of a VBE is obtained as follows [3]:

$$I_c > 0.00307 t_w h^4 / L \quad (2)$$

Where I_c denotes the VBE moment of inertia, and t_w, h, and L are the thickness, height, and length of the web plate, respectively. If h replaces L, Eq. (2) can be used for HBEs. Specimens were designed considering the limited maximum allowable load and the specimen size in the lab. Fig. 2 shows the details of the designed specimens, HBE and VBE sections. HBE and VBE plates were connected using full-penetration groove welding. Two beams were executed at the top level of the specimens parallel to the HBE on both sides as lateral restraints to prevent out-of-plane movement. The base VBE was connected to the floor HBE using full-penetration welding, and the welding connection to the flange of the HBE was according

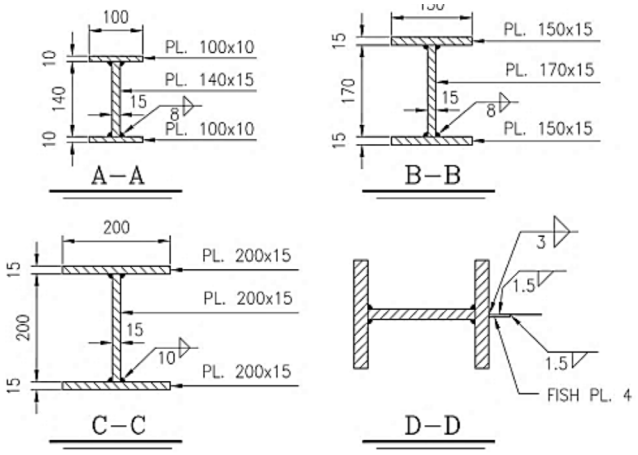

Fig. 2 HBE and VBE sections (mm): (a) Section top HBEs, (b) Section VBEs, (c) Bottom HBE, and (d) Details of fish plate connection to the boundary elements. (Note. HBE: Horizontal boundary element; VBE: Vertical boundary element)

to the design load. An equilateral triangular reinforcing plate with a leg length of 200 mm and a thickness of 10 mm was added to the VBE floor HBE connection to transfer the VBE concentrated load to the floor HBE at a greater length to prevent the floor HBE web-to- flange connection rupture. In addition, VBEs were connected to the lower HBE and VBE using the full-penetration groove welding of the flanges and the corner welding of the web and connection plates to establish a full-grip connection. Subsequently, the specimens were groove-welding quality control and penetration test for welds were performed according to the AWS, VT (for visual inspection), and PT (for penetrating liquid inspections) standards.

A deep H-shaped HBE was used to connect the steel shear wall to the lab's strong floor. Further, the specimens were connected using M24 high-strength bolts and nuts by attaching the lower flange of the lower HBE to the strong floor of the lab (Fig. 3).

2.2 Properties of the materials

The ST37 steel [34] was employed for the web plate and boundary elements of all specimens. A tension coupon test determined the mechanical properties (Table 1) [35]. Three specimens were tested for each plate thickness.

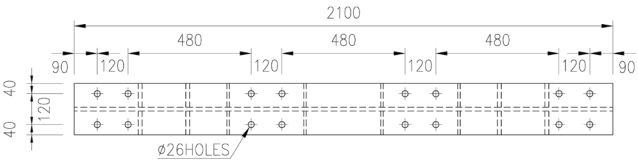

Fig. 3 Bottom HBE connection details (mm)

Table 1 Mechanical properties

Type	Steel DIN Germany Standard	Young's Modulus E (GPa)	Yield Stress f_y (MPa)	Ultimate Stress f_u (MPa)	f_u/f_y
Web Plate (pl 0.5 mm)	ST37	210	230	310	1.34
Web Plate (pl 1.5 mm)	ST37	210	242	339	1.40
Fish Plate (pl 4 mm)	ST37	210	260	374	1.43
VBEs and HBEs (pl 10 mm)	ST37	210	350	425	1.21
VBEs and HBEs (pl 15 mm)	ST37	210	380	480	1.26

2.3 Test setup

After fabrication and before loading, the surfaces of all four specimens were covered with a hydrated lime solution to observe their behavior during loading. Fig. 4 illustrates the set up that provides lateral support for the upper HBE and prevents out-of-plane deformations.

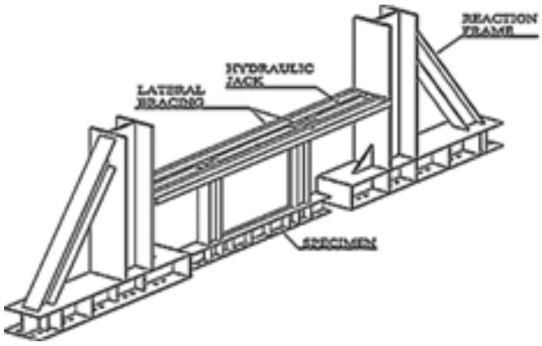

(a)

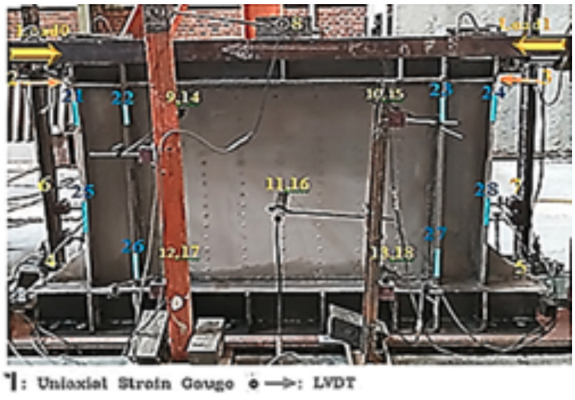

(b)

Fig. 4 Test setup: (a) Schematic test setup, (b) Position of LVDTs and strain gauges on specimens (Note. LVDT: Linear variable differential transformer)

2.3.1 Cyclic loading test

A quasi- static cyclic loading with increasing load and displacement was used to simulate the earthquake load and analyze the behavior of specimens in each cycle. Moreover, ATC-24 displacement control protocol [36], which was developed for steel-structure members, was employed to evaluate the seismic behavior of the specimens based on the loading history. The amounts of which corresponded to the specimen yield (Δ_{yield}). The loading was applied on the upper HBE. The maximum horizontal displacement at the top of specimens was measured as follows (Fig. 5).

The loading history was interrupted with small cycles, after every three cycles of loading with displacement equal to or larger than the yield displacement based on the ATC-24 recommendation. These small cycles were force controlled using a peak value of 0.75 of the force that causes the occurrence of yielding.

Two 1200-kN hydraulic jacks were located on each side of the top of the wall for imposing the lateral loads. Two load cells were placed between hydraulic jacks and loading frames for recording the lateral forces. Two linear variable differential transducers (LVDTs) were utilized at the top level of the wall to measure the displacements during the tests. Similarly, LVDTs and strain gauges were used to measure the amount of deformation and strain at the other points of the specimens where measurements were recorded by a data logger (Fig. 4).

3 Analysis of the test results

This section studies differences in mechanical characteristics and properties, including elastic and effective stiffness, maximum base shear, ductility, energy absorption, ultimate strength, and failure modes, and distinguishes the seismic behavior of different configurations of SPSWs.

3.1 SPSW specimen

In this specimen, the first web plate permanent buckling occurred in cycle 11 with 7.7 mm displacement (0.7% drift), and yielding began in the VBE's outer flange near the

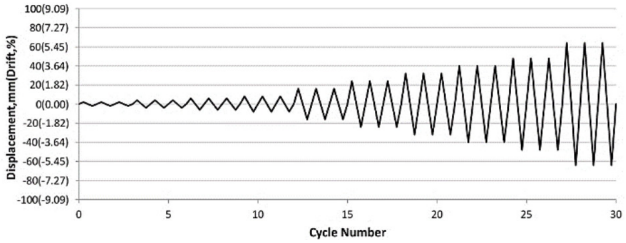

Fig. 5 Loading pattern

gusset connection to the VBE (Fig. 6(b)). In cycle 23 with 22.55 mm lateral displacement (2.05% drift), the first tear was detected at the top left corner of the infill plate (Fig. 6(c)). Them, puncture occurred after the complete yielding of the web plate. The failure of the upper HBE flange next to the connection to the VBE and failure of the connection to the VBE, yielding of the VBE flange, rupture of the weld of the web plate to the fish plate, and tearing at the top edge of the triangular sheet of joint reinforcement were observed by continuing the loading.

The highest shear capacity was 900 kN in the 19th loading cycle in the 31.24 mm displacement (2.84% drift, Fig. 6(d)). VBE flange separation occurred near the upper edge of the triangular connection-strengthening plate in the 72.71 mm displacement (6.61% drift, Fig. 6(e)). Loading continued up to the 79.09 mm displacement (7.19% drift, Fig. 6(f)). The behavior of the specimen was linear up to the displacement of 7.15 mm, and the load at this stage was 714 kN. The hysteresis curves are spindle-shaped and symmetrical. The hysteresis curve of the specimen shows that there is no decrease in strength during the cycles, but the stiffness of the web plate decreases in each loading cycle. (Fig. 6(a)).

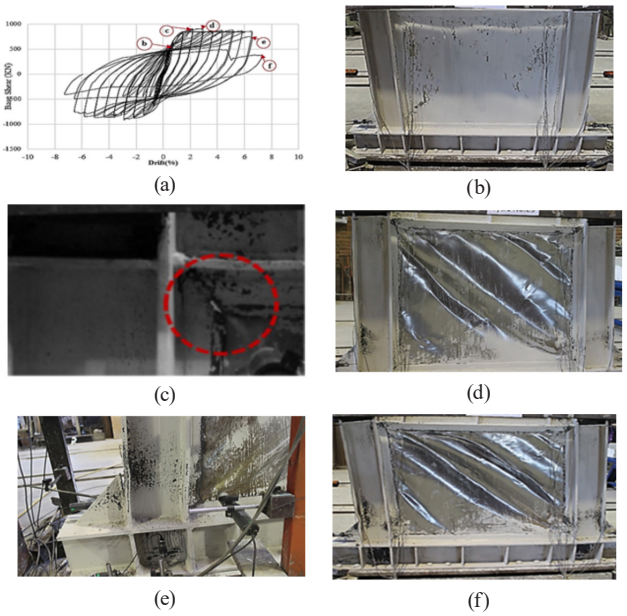

Fig. 6 Specimen 1 (SPSW) lateral load-drift response and buckling pattern: (a) Lateral load-drift response, (b) Buckling permanent in the web plate at 0.70% drift, (c) The first tear in the web-plate corner in cycle 23 and 2.05% drift, (d) At 2.84% drift in cycle 19, (e) VBE flange separation near the upper edge of the triangular connection-strengthening plate at 6.61% drift, and (f) The end of the test at 7.19% drift

3.2 CSPSW specimen

In this specimen, the corrugated plate yielding occurred in cycle 4 with 4 mm displacement (0.36% drift). In cycle 11, with 8 mm displacement (0.73% drift(, the welding fracture of the corrugated plate started from the connection between the plate and VBEs, and the web plate rupture began around the welds due to crippling (Fig. 7(b)). In cycle 20, with 24 mm displacement (2.18% drift), local and general buckling was observed on the web plate, and the connection welding broke from the VBE flange and the corner of the connecting plate to the HBE. As the shear wall was still able to bear loads, loading continued (Fig. 7(c)) until the weld between the VBE and the lower beam broke. The failure and tearing of the web plate of the fish plate, the yielding of the VBE flange, the breaking of the weld of the web plate to the fishplate, and the deformation of the trapezoidal corrugated plate next to the VBE, and finally, the failure of the stiffeners lower beam (under the VBE) were observed by continuing the loading.

The highest shear capacity of this specimen was 766.5 kN and was observed in cycle 18 with 18 mm displacement (1.64% drift). The loading was terminated in cycle 28 with 50 mm displacement (4.54% drift). Fig. 7(d)) depicts the specimen at the end of loading. The behavior of the

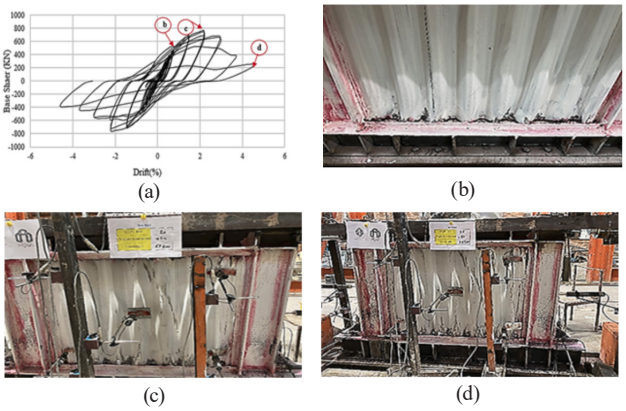

Fig. 7 Specimen 2 (CSPSW) lateral load-drift response and buckling pattern: (a) Lateral load-drift response, (b) Failure of the weld of the corrugated plate from the connection plate at 0.73% drift, (c) Buckling permanent in the web plate at 2.18% drift, and (d) The end of the test at 4.54% drift

specimen was linear up to the displacement of 5.17 mm, and the load at this stage was 580 kN. Moreover, hysteresis curves were S-shaped, and the middle of the curve showed necking. The hysteresis curve of the specimen demonstrated the decrease of stiffness, strength of the web plate of the shear wall, and thus the occurrence of the shrinkage. Therefore, the area under the curve decreased by decreasing stiffness and strength, leading to a great reduction in the energy dissipation of the specimen (Fig. 7(a)).

3.3 SCSSPSW specimen

In this specimen, the web plates buckling occurred permanently at cycle 16 with 16 mm displacement (1.45% drift), and self-tapping screws started to pull out from one of the web plates (Fig. 8(b)). In cycle 21, with 32 mm displacement (2.90% drift), the first perforation started from the corner of the web plate near the HBE to VBE connection and continued after the web plate yielded and underwent large deformations. As loading continued, the welding between VBE cracked and detached from it, and the welding between web plate and fishplate cracked, causing the screws of the web plate pull out from their places. In 40 mm displacement (3.6% drift), the rift started from the location of screws on the web flat plates, and in 50 mm displacement (4.5% drift), the self-screw holes cracked in the vertical and horizontal rows near the HBE and VBE. The fish plate and web plate cracked. The all of self-tapping screws on one of the web plates pull out, and the web plate tore. The loading was terminated in cycle 30 with 54 mm (4.9% drift). The highest shear capacity 880 KN occurred in cycle 21 with 22.55 mm displacement (2.05% drift) (Fig. 8(c)). Fig. 8(d) Shows the specimen at the end of the loading. Loading continued up to the 61.93 mm displacement (5.63% drift), (Fig. 8(d)).

The behavior of the specimen was linear up to the displacement of 8.2 mm, and the load at this stage was 633 kN, hysteresis curves were asymmetric S-shaped, and the middle of the curve shows necking. The hysteresis curve of the specimen showed decrease of stiffness, strength of the web plate of the steel shear wall, and shrinkage had occurred. Therefore, by decreasing the stiffness and strength, the area under the curve decreased and the energy dissipation of the specimen was greatly reduced; (Fig. 8(a)).

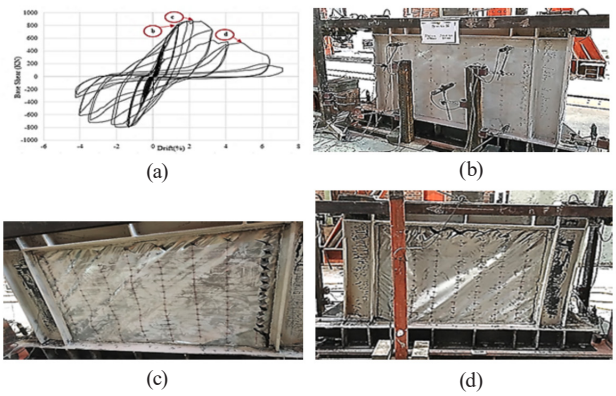

(a) (b) (c) (d)

Fig. 8 Specimen 3 (SCSSPSW) lateral load-drift response and buckling pattern: (a) Lateral load-drift response, (b) Buckling permanent in the web plate at 1.45% drift, (c) The highest shear capacity at 2.90% drift, and (d) The end of the test at 5.63% drift

3.4 CSCSPSW specimen

In this specimen, the web plate began to yield in cycle 4 with 4 mm displacement (0.36% drift). The first web plate permanent buckling occurred in the cycle 7 with 6 mm displacement (0.54% drift), deformation of the first trapezoidal wave occurred next to the VBE, and in cycle 12 with 8 mm displacement (0.73% drift), yielding began in the VBE outer flange and deformation increased on the trapezoidal web plate (Fig. 9(b)).

In cycle 14 with 16 mm displacement (1.45%) drift, the vicinity of the first bolt that connected the trapezoidal plate to the fish plate was deformed, and yielding was observed in the foot of the VBE. In cycle 18, with 24 mm displacement (2.18% drift), the webs of VBEs underwent horizontal and angular yielding with general and local buckling and deformation in the web plate.

In cycle 23 with 30.8 mm displacement (2.80% drift) (Fig. 9(c)), all the web-plate bottom trapezoidal corrugated plates were deformed from trapezoidal to sinusoidal. In cycle 25 with 40 mm displacement (3.64% drift), buckling in the trapezoidal corrugated web plate happened and the first perforation occurred, and the top of the web plate cracked near that bolt connected to the fish plate (Fig. 9(d)). In cycle 29 with 55 mm displacement (5.00% drift), the welding at the VEB foot failed at the VEB connection. The web plate's top first-row bolt detached from

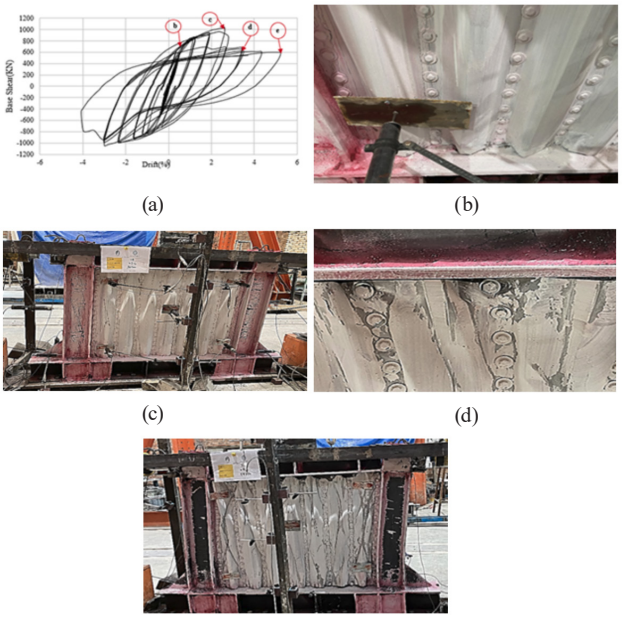

(a) (b) (c) (d) (e)

Fig. 9 Specimen 4 (CSCSPSW) lateral load-drift response and buckling pattern: (a) Lateral load-drift response, (b) Buckling permanent in the web plate at 0.73% drift, (c) Replacement 1000 KN jack at 2.80% drift, (d) At 3.64% drift in cycle 25, and (e) The end of the test 5.00% drift

Table 2 The web plate permanent buckling in the specimens

Specimen		SPSW		CSPSW		SCSSPSW		CSCSPSW	
		Drift (%)	Load (kN)	Drift (%)	Load (kN)	Drift (%)	Load (kN)	Drift (%)	Load (kN)
+	First web plate permanent buckling	0.7	641.61	0.54	587.3	1.4	809.46	1.45	898.1
-		0.73	632.6	0.44	573.9	1.37	788.54	1.65	889.11
Average		0.72	637.10	0.49	580.60	1.39	799	1.52	893.61
+	Maximum load	2.9	890.14	1.64	770.76	2.17	881.76	2.61	1044.6
-		2.78	909.86	1.57	762.24	1.92	878.24	2.99	1057.4
Average		2.84	900	1.61	766.50	2.05	880	2.80	1051
+	End of loading	7.25	322.31	4.53	231.43	7.11	125.21	5.21	594.74
-		7.13	404.14	4.56	389.28	4.15	223.44	4.79	457.21
Average		7.19	363.22	4.54	310.35	5.63	174.32	5.00	525.98

the connecting plate, and perforation was observed in four areas in the trapezoidal web plate (Fig. 9(e)). In this specimen, the highest shear capacity 1050 KN occurred in cycle 25 with 40 mm displacement (3.64% drift) (Fig. 9(d)). The loading was continued cycle 29 with 55 mm (5.00% drift). Fig. 9(e) shows the specimen at the end of the test. The behavior of the specimen was linear up to the displacement of 6.20 mm, and the load at this stage was 708 kN, and from this stage, the non-linear behavior of the specimen started, and residual deformations remained in the specimen. Hysteresis curves were symmetric S-shaped, the more area under the curve shows the more flexibility and energy dissipation of the specimen (Fig. 9(a)).

The maximum lateral loads and the specimens' first web plate permanent buckling are reported in Table 2 and depicted in Figs. 6 to 9.

The buckling strength of the web plate increased in the CSCSPSW specimen compared to the other specimens. Tensile buckling in the proposed specimen was observed diagonally in each wave of the trapezoidal corrugated sheet, and the observed out-of-plane buckling in VBEs was less than the other specimens at the end of the test. The puncture of the corrugated plate occurred after the complete yielding of the web sheet and large deformations.

3.5 Idealized force–deformation curve

The ASCE41-17 [37] specified method was used for determining the linear curve of the specimen's behavior to obtain and compare their structural properties, including effective stiffness, yield and ultimate strength, ductility, and performance parameters.

Elastic stiffness (K_0) and effective stiffness (K_e) were the other important specimen parameters, which were found from the slope of the elastic part of the curve and the first line of the bilinear force displacement curve, respectively (Fig. 10).

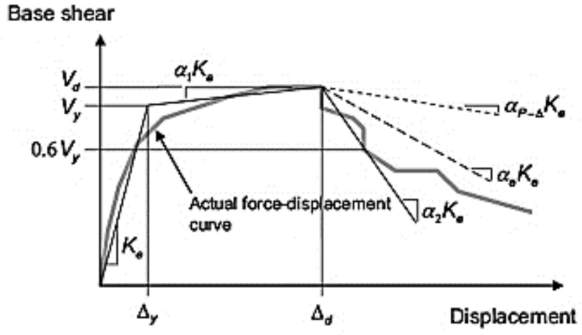

Fig. 10 The idealized force-displacement curve of ASCE41-17 [37]

Based on ASCE41-17 [37], the bilinear force-displacement curve was fitted on each specimen's backbone curve, and the comparison of backbone curves is illustrated in Figs. 11(a) to 11(e).

As shown in Fig. 11(f), the mean values of cumulative energy dissipations for specimen CSCSPSW with 44 mm displacement (4% drift) are about 3, 57, and 32% more than those of SPSW, CSPSW, and SCSSPSW, respectively.

Fig. 11 Idealized backbone curves obtained from the test of specimens according to ASCE41-17.: (a) specimen SPSW, (b) specimen CSPSW, (c) specimen SCSSPSW, (d) specimen CSCSPSW, (e) The lateral force-drift ratio (The backbone curve), (f) The dissipated energy of the specimens

The coefficient m-factor suggested by ASCE41-17 [37] is a modification factor to consider the expected ductility of the member at each structural performance level calculated using the bilinear curve obtained from the lab characteristic curve results. To find this coefficient, it is necessary to specify the displacement at each performance level. Three performance levels, including immediate occupancy (IO), life safety (LS), and collapse prevention (CP), should be taken into consideration. According to Eq. (3), displacement at the collapse prevention level (δ_{CP}) equals that of the bilinear curve at the maximum base

shear. At his level, minor stiffness and strength remain to withstand the lateral loads, and deformations have long durability. Displacement at the life safety level (δ_{LS}) equals 0.75 δ_{CP} based on Eq. (4). At this level, the system shows relative deformation due to plastic behavior. Finally, displacement at the immediate occupancy level (δ_{lo}) equals the displacement where the first permanent visible damage (crack) occurs in the lab specimen; according to Eq. (5), it should not exceed 0.67 δ_{LS}. Yield displacement (δ_y) is related to the specimen's yield point. At each performance level, coefficient m displacement equals the displacement of that same level divided by the yield point.

δ_{IO} is the displacement related to the first observed damage at experimental specimens; it should not exceed 67% of the life safety displacement. The ASCE41-17 method was employed to obtain the idealized force–deformation curves (Fig. 11). After the curves were bi-linearized, the ductility modification factor (m) was found for the specimens (Table 3).

$$m_{CP} = \frac{\delta_{CP}}{\delta_y} \tag{3}$$

$$m_{LS} = \frac{\delta_{LS}}{\delta_y},\ \delta_{LS} = 0.75\delta_{CP} \tag{4}$$

$$m_{IO} = \frac{\delta_{IO}}{\delta_y} \tag{5}$$

In Fig. 11, the solid lines are the lateral load-drift ratio curves of the specimens, and the dashed lines are the idealized curves. The component capacity modification factor (m-factors), the elastic stiffness, the effective stiffness, the effective yield strength, and the maximum base shear of the specimens are presented in Tables 3 and 4. Based on the findings (Table 3), the mean values of the m-factors of specimen CSCSPSW, compared to those of specimens SPSW, CSPSW, and SCSSPSW, increased by about 4, 5, and 10%, as well as 35, 40, and 43 compared to the SPSW and CSPSW specimens, and 71, 70, and 79% in comparison to SCSSPSW at the performance levels of IO, LS, and CP, respectively.

According to the results obtained from the idealized force–deformation curves, the m-factors, effective stiffness, effective yielding force, and the maximum lateral load of trapezoidal corrugated plates increased compared to the other specimens. Table 4 indicates that the mean values of the elastic stiffness for specimen CSCSPSW, compared to those of specimens SPSW, CSPSW, and SCSSPSW, increased by around 46, 10, and 131%, respectively. In contrast, the mean values of the effective stiffness for the CSCSPSW specimen increased by about 20, 6, and 56%, respectively, compared to specimens SPSW, CSPSW, and SCSSPSW. Additionally, the maximum lateral load capacity of specimen CSCSPSW increased by nearly 17, 37, and 19%, respectively, compared to those of SPSW, CSPSW, and SCSSPSW specimens. The mean values of the yield strength specimen CSCSPSW were equal to that of SPSW and were about 22% and 12% more than those of CSPSW and SCSSPSW, respectively.

The reason for increasing the initial and effective stiffness of the proposed specimen, compared to other ones, was the presence of two corrugated plates with a higher stiffness than the flat plate and the shape of its placement. Considering that trapezoidal corrugated plates had a special geometry and out-of-plane stiffness, they have a much higher buckling resistance than the flat plate because their multiple bends converted in-plane forces into out-of-plane

Table 3 The m-factors calculated from the idealized force – deformation curve of specimens

Specimen	SPSW	CSPSW	SCSSPSW	CSCSPSW
+	mCP	3.35	2.45	2.03
-		3.32	2.68	2.06
Average		3.34	2.56	2.05
+	mLS	2.53	1.84	1.54
-		2.49	2.01	1.54
Average		2.51	1.93	1.54
+	mIO	1.69	1.25	1.03
-		1.67	1.35	1.03
Average		1.68	1.30	1.03

Table 4 The elastic and effective stiffness and yield and ultimate strength of the specimens

Specimen		SPSW	CSPSW	SCSSPSW	CSCSPSW
+	Elastic stiffness (KN/mm) K_0	132.76	134.29	76.21	143.44
-		95.02	168.36	67.67	188.94
Average		113.89	151.32	71.94	166.19
+	Effective stiffness (KN/mm) K_e	102.37	106.75	77.25	100.08
-		97.55	118.55	76.23	139.78
Average		99.96	112.64	76.74	119.93
+	Maximum lateral load capacity (KN) V_{max}	890.14	770.76	881.76	1044.61
-		909.86	762.24	878.24	1057.39
Average		900	766.12	880	1051
+	Yield strength (KN) V_y	732	587.3	679.8	660
-		697.5	573.9	647	725.55
Average		714	580.60	633.40	708

forces and vice versa. The inherent geometric stiffness of the corrugated plate eliminates problems associated with out-of-plane buckling. In addition, the proper connection of all three web plates to each other with bolts and nuts was maintained until the end of the test of this connection. In CSPSW, due to the high stiffness of the shear wall, the boundary elements experienced premature failure in lower HBE connections. In SCSSPSW, the three plates were not fully connected with self-tapping screws; therefore, the plates acted separately, and the stiffness of the specimen represented a great reduction. Due to the low thickness of the wall sheet, failure and tearing occurred at the location of self-tapping screws. Thus, the web sheet did not enter the post-buckling stage. The high initial and effective stiffness of CSCSPSW was due to the presence of two corrugated plates with a higher stiffness than the flat sheet. Further, the proper connection of all three webs to each other by bolts was maintained until the end of the test.

Given that the web sheet's bearing share in the prototype design is considered 35% of the whole system with a flat plate, the stiffness created in the steel shear wall system is highly important. Increasing the stiffness of the wall webs significantly affects the strength of the system, changes the failure mode to shear failure and reduces the required stiffness resistance of the boundary members. The high stiffness of the specimen caused a decrease in the drift ratio.

The stiffness of the proposed system and its final shear strength increased compared to the other specimens. This is because placing two corrugated plates on the two sides of the flat plate increased the web plate's buckling strength, delayed the formation of tension fields in the web plate, and adjusted the stresses until reaching the final load compared to the other specimens. Due to the buckling of the corrugated plates, trapezoidal plates changed into a sinusoidal shape, leading to an increase in the post-buckling resistance.

In the proposed CSCSPSW specimen, less damage happened in VBEs and HBEs, implying an increase in the share of the web plate in the total capacity of the steel shear wall system.

Local and global buckling happened in the corrugated plates of CSCSPSW specimens. The elastic shear strength was reduced because of these buckling effects, while the ultimate and post-buckling strength increased. Then, the final strength of the corrugated plate happened when flat plates reached the yield point or underwent local buckling; in fact, flat plates provided the source of post-buckling strength for the entire corrugated plate. In the global buckling mode, the plate shear strength was reduced because that buckling began in the corrugated plate, expanded all around, and changed the plate geometry. Therefore, contrary to the web plate of the unstiffened steel shear wall, where the defect was detected only on the diameter, it spread all over the corrugated plate.

3.6 Ductility coefficient

Seismic load-bearing structures that can withstand non-elastic deformations at a certain section without significantly reducing strength and stiffness against reciprocating loads were considered ductile, and their ductility coefficient (μ) was calculated by Eq. (6). Table 5 presents the ductility coefficient of the specimens.

$$\mu = \frac{\Delta_{\max}}{\Delta_y} \tag{6}$$

The ductility coefficient of specimen CSCSPSW increased by around 12, 50, and 82% compared to SPSW, CSPSW, and SCSSPSW specimens, respectively. Due to its geometry, the CSCSPSW specimen had higher stiffness and ductility than the flat plates. In SCSSPSW specimens, failure occurred at the location of self-tapping screws, and the wall did not enter the post-buckling stage.

Due to the presence of two flat plates and one corrugated plate with low thickness in the SCSSPSW, it was expected to show more ductility, but owing to the lack of complete connection of the three plates with self-tapping screws, the plates acted separately and reduced the ductility of the specimen. Due to the low thickness of the flat plates, more failure and tearing occurred at the place of the self-tapping screws; thus, the specimen did not enter the post-buckling stage.

Table 5 Specimens' ductility coefficients found based on the test result information

Specimen		SPSW	CSPSW	SCSSPSW	CSCSPSW
+	Yield displacement Δ_y (mm)	7.15	5.5	8.8	5.92
-		7.15	4.84	7.7	6.48
Average		7.15	5.17	8.25	6.2
+	Maximum displacement Δ_{max} (mm)	31.92	17.97	23.87	28.69
-		31.63	17.30	21.08	32.97
Average		31.77	17.36	22.48	30.83
+	Ductility ($\Delta_{max}\Delta_y$)	4.46	3.15	2.72	4.85
-		4.42	3.57	2.75	5.09
Average		4.44	3.36	2.73	4.97

In CSCSPSW, due to the combination of two trapezoidal corrugated plates with a flat plate and the way they are attached to each other, and the fish plate, higher stiffness and ductility happened in comparison to the other specimens. It must be mentioned that some of the reasons for decreasing the ductility of the CSPSW specimen were the breakage of the stiffener at the VBE foot and the failure of the entire system.

4 Summary and conclusions

This study investigated and compared the performance of four one-third-scale specimens under cyclic loading. Specimens were studied with optimal designs in the HBEs and VBEs of specimens. As the steel shear wall is an essential system in seismic issues, the perimeter frame was designed in all specimens based on a special, high-ductility, flexural, dual, I-section frame system, and the sections of all boundary members (HBEs and VBEs) were assumed fixed to compare the seismic performance of specimens. Triangular plates were used at the column base connection to prevent failure due to high axial force, and in the analytical models, it was clear that stress concentration was distanced from the VBE base by using these plates.

The ST37 steel was employed for all specimens' web plates and boundary elements. Steel shear wall specimens included an unstiffened specimen (SPSW), a specimen with a vertical 45° trapezoidal corrugated web (CSPSW); the specimen with a corrugated web plate, reinforced with two flat plates, and the specimen with a flat web plate, reinforced with two corrugated plate (CSCSPSW). The web plate thickness was 1.5 mm in all specimens. A 40 × 4 mm fish plate was applied to connect the web plates to the surrounding frame. It is worth mentioning that the number of tests is limited and pilot program. Thus, more tests are required to ensure the accuracy of conclusions. The main results are as follows:

- Among the tested specimens, the maximum load-bearing capacity was related to CSCSPSW due to the proper connection of three plates and the placement of two corrugated plates with the flat web plate.
- The maximum initial and effective stiffness was related to specimen CSCSPSW because the trapezoidal corrugated plates had much higher buckling resistance than flat ones due to their special geometry and off-plane stiffness. Corrugated plates restrained each other because the multiple bends in the plate converted in-plane forces to out-of-plane and vice versa. Due to their inherent geometric stiffness, corrugated plates were stiffer. This was quite evident in different specimen test.
- The lowest initial and effective stiffness belonged to specimen SCSSPSW due to the lack of complete connection between screws and plates. Therefore, each plate reacted separately. The failure happened at the places of screws due to their low thicknesses; buckling did not happen, causing stiffness reduction.
- Specimen CSCSPSW had the maximum base shear. In SCSSPSW, self-tapping screws were loosened in the inelastic deformation range, the three plates lose their connection, and the seismic behavior decreased. The failure mainly occurred at the location of self-tapping screws, and rupture occurred on plates; the specimen did not enter the post-buckling stage. Here, the column foot weld quickly broke due to the force transferred from the steel shear wall to the frame.
- Despite its high stiffness, specimen CSCSPSW had more acceptable ductility than other specimens. In specimen CSCSPSW, the initial and effective stiffness, ductility coefficient, strength, and maximum base shear increased because the steel shear wall had the same web plate thickness, which reduced the load-bearing capacity of the boundary elements and prevented elastic buckling.
- The proper connections of the VBE base to the floor HBE and proper VBE stiffness could increase the energy dissipation capacity; however, in large-drift displacements, this capacity might slightly reduce due to the strengthening of the corrugated plate on the web plate and vice versa.

In general, specimen CSCSPSW demonstrated better and more stable behavior during loading and improved the weaknesses related to the seismic performance of unstiffened and trapezoidal corrugated steel shear walls with similar thicknesses and materials. As already mentioned, the number of tests was limited in this study, and more research is needed to provide a comprehensive understanding of the performance of steel plate shear walls reinforced with trapezoidal corrugated plates in improving the seismic behavior of different structural members.

References

[1] Driver, R. G., Kulak, G. L., Kennedy, D. J. L., Elwi, A. E. "Cyclic Test of Four-Story Steel Plate Shear Wall", Journal of Structural Engineering, 124(2), pp. 112–120, 1988. https://doi.org/10.1061/(ASCE)0733-9445(1998)124:2(112)

[2] ASCE "Minimum Design Loads for Buildings and Other Structures: ASCE/SEI 7-10", American Society of Civil Engineers, Reston, VA, USA, 2013. ISBN: 9780784412916 https://doi.org/10.1061/9780784412756

[3] ANSI "Seismic Provisions for Structural Steel Buildings (ANSI/AISC 341-10)", Washington, DC, USA, 2010.

[4] AISC "Steel Design Guide 20. Steel Plate Shear Walls", American Institute of Steel Construction, Chicago, IL, USA, 2007.

[5] Berman, J. W., Celik, O. C., Bruneau, M. "Comparing hysteretic behavior of light-gauge, steel plate shear walls and braced frames", Engineering Structures, 27(3), pp. 475–485, 2005. https://doi.org/10.1016/j.engstruct.2004.11.007

[6] Berman, J. W, Bruneau, M. "Experimental investigation of light-gauge steel plate shear walls", Journal of Structural Engineering, 131(2), pp. 259–267, 2005. https://doi.org/10.1061/(ASCE)0733-9445(2005)131:2(259)

[7] Easley, J. T. "Buckling formulas for corrugated metal shear diaphragms", Journal of the Structural Division, 101(7), pp. 1403–1417, 1975. https://doi.org/10.1061/JSDEAG.0004095

[8] Easley, J. T., McFarland, D. E. "Buckling of light-gage corrugated metal shear diaphragms", Journal of the Structural Division, 95(7), pp. 1497–1516, 1969. https://doi.org/10.1061/JSDEAG.0002313

[9] Tong, J.-Z., Guo, Y.-L. "Shear resistance of stiffened steel corrugated shear walls", Thin-Walled Structures, 127, pp. 76–89, 2018. https://doi.org/10.1016/j.tws.2018.01.036

[10] Dou, C., Pi, Y.-L., Gao, W. "Shear resistance and post-buckling behavior of corrugated panels in steel plate shear walls", Thin-Walled Structures, 131, pp. 816–826, 2018. https://doi.org/10.1016/j.tws.2018.07.039

[11] Dou, C., Jiang, Z.-Q., Pi, Y.-L., Guo, Y.-L. "Elastic shear buckling of sinusoidally corrugated steel plate shear wall", Engineering Structures, 121, pp. 136–146, 2016. https://doi.org/10.1016/j.engstruct.2016.04.047

[12] Feng, L., Sun, T., Ou, J. "Elastic buckling analysis of steel-strip-stiffened trapezoidal corrugated steel plate shear walls", Journal of Constructional Steel Research, 184(2), 106833, 2021. https://doi.org/10.1016/j.jcsr.2021.106833

[13] Emami, F., Mofid, M., Vafai, A. "Experimental study on cyclic behavior of trapezoidal corrugated steel shear walls", Engineering Structures, 48, pp. 750–762, 2013. https://doi.org/10.1016/J.ENGSTRUCT.2012.11.028

[14] Vigh, L. G., Deierlein, G. G., Miranda, E., Liel, A. B., Tipping, S. "Seismic performance assessment of steel corrugated shear wall system using non-linear analysis", Journal of Constructional Steel Research, 85, pp. 48–59, 2013. https://doi.org/10.1016/j.jcsr.2013.02.008

[15] Vigh, L. G., Liel, A. B., Deierlein, G. G., Miranda, E., Tipping, S. "Component model calibration for cyclic behavior of a corrugated shear wall", Thin-Walled Structures, 75, pp. 53–62, 2014. https://doi.org/10.1016/j.tws.2013.10.011

[16] Emami, F., Mofid, M. "On the hysteretic behavior of trapezoidal corrugated steel shear walls", Structural Design of Tall and Special Buildings, 23, pp. 94–104, 2014. https://doi.org/10.1002/tal.1025

[17] Guo, T., Sause, R. "Analysis of local elastic shear buckling of trapezoidal corrugated steel webs", Journal of Constructional Steel Research, 102, pp. 59–71, 2014. https://doi.org/10.1016/j.jcsr.2014.06.006

[18] Hosseinpour, E., Baharom, S., Yadollahi, Y. "Evaluation of steel shear walls behavior with sinusoidal and trapezoidal corrugated plates", Advances in Civil Engineering, 2015, 715163, 2015. https://doi.org/10.1155/2015/715163

[19] Yadollahi, Y., Pakar, I., Bayat, M. "Evaluation and comparison of behavior of corrugated steel plate shear walls", Latin American Journal of Solids and Structures, 12(4), pp. 763–786, 2015. https://doi.org/10.1590/1679-78251469

[20] Farzampour, A., Laman, J. A., Mofid, M. "Behavior prediction of corrugated steel plate shear walls with openings", Journal of Constructional Steel Research, 114, pp. 258–268, 2015. https://doi.org/10.1016/j.jcsr.2015.07.018

[21] Kalali, H., Ghanbari Ghazijahani, T., Hajsadeghi, M., Zirakian, T., Alaee, F. J. "Numerical study on steel shear walls with sinusoidal corrugated plates", Latin American Journal of Solids and Structures, 13(15), pp. 2502–2514, 2016. https://doi.org/10.1590/1679-78252837

[22] Bahrebar, M., Kabir, M. Z., Zirakian, T., Hajsadeghi, M., Lim, J. B. P. "Structural performance assessment of trapezoidally-corrugated and centrally-perforated steel plate shear walls", Journal of Constructional Steel Research, 122, pp. 584–594, 2016. http://doi.org/10.1016/j.jcsr.2016.03.030

[23] Bahrebar, M., Kabir, M. Z., Hajsadeghi, M., Zirakian, T., Lim, J. B. P. "Structural performance of steel plate shear walls with trapezoidal corrugations and centrally-placed square perforations", International Journal of Steel Structures, 16, pp. 845–855, 2016. https://doi.org/10.1007/s13296-015-0116-y

[24] Yu, C., Yu, G. "Experimental investigation of cold-formed steel framed shear wall using corrugated steel sheathing with circular holes", Journal of Structural Engineering, 142(12), 04016126, 2016. https://doi.org/10.1061/(ASCE)ST.1943-541X.0001609

[25] Zhang, W., Mahdavian, M., Li, Y., Yu, C. "Experiments and simulations of cold-formed steel wall assemblies using corrugated steel sheathing subjected to shear and gravity loads", Journal of Structural Engineering, 143(3), 04016193, 2017. https://doi.org/10.1061/(ASCE)ST.1943-541X.0001681

[26] Jiang, Z., Yang, X.-F., Dou, C., Li, C., Zhang, A. "Cyclic testing of replaceable damper: earthquake-resilient prefabricated column-flange beam-column joint", Engineering Structures, 183, pp. 922–936, 2019. https://doi.org/10.1016/J.ENGSTRUCT.2019.01.060

[27] Guo, Y.-L., Zhu, J.-S., Wang, M.-Z., Yang, X., Zhou, P. "Overall instability performance of concrete-infilled double steel corrugated-plate wall", Thin-Walled Structures, 130, pp. 372–394, 2018. https://doi.org/10.1016/j.tws.2018.05.026

[28] Zhu, J.-S., Guo, Y.-L., Wang, M.-Z., Yang, X., Zhu, B.-L. "Strength design of concrete-in filled double steel corrugated-plate walls under uniform compressions", Thin-Walled Structures, 141, pp. 153–174, 2019. https://doi.org/10.1016/j.tws.2019.02.021

[29] Jiang, Z.-Q., Yan, T., Zhang, A.-L., Su, L., Shen, C.-J. "Experimental research on special steel frame with stiffened double steel plate shear wall", Journal of Constructional Steel Research, 189, 107067, 2022. https://doi.org/10.1016/j.jcsr.2021.107067

[30] Tong, J.-Z., Guo, Y.-L., Zuo, J.-Q., Gao, J.-K. "Experimental and numerical study on shear resistant behavior of double-corrugated-plate shear walls", Thin-Walled Structures, 147, 106485, 2019. https://doi.org/10.1016/j.tws.2019.106485

[31] "AC 154. Acceptance Criteria for Cyclic Racking Shear Tests for Metal-Sheathed Shear Walls with Steel Framing", ICC Evaluation Service, 2008.

[32] ASTM "ASTM C1513-18. Standard Specification for Steel Tapping Screws for Cold-Formed Steel Framing Connections", ASTM International, West Conshohocken, PA, USA, 2018. https://doi.org/10.1520/C1513-18

[33] Sabelli, R., Bruneau, M. "Design Guide 20: Steel Plate Shear Walls", American Institute of Steel Construction (AISC), Chicago, IL, USA, 2007.

[34] DIN "1623 Cold rolled strip and sheet - Technical delivery conditions - General structural steels", German Institute for Standardization, Berlin, Germany, 1983.

[35] ASTM "ASTM A370-12 Standard Test Methods and Definitions for Mechanical Testing of Steel Products", ASTM International, West Conshohocken, PA, USA, 2012. https://doi.org/10.1520/A0370-12

[36] ATC "ATC-24. Guidelines for Cyclic Testing of Components of Steel Structures", Applied Technology Council, Redwood City, CA, 1998.

[37] ASCE "ASCE/SEI 41-17 Seismic Evaluation and Retrofit of Existing Buildings", American Society of Civil Engineers, Reston, VA, USA, 2017. https://doi.org/10.1061/9780784414859